Title
Bifurcation Analysis of Sub-Synchronous Oscillations Related to Grid-Forming Converter Inner Controllers

Journal
Proceedings of the PowerUp Conference, 1(1)

Authors
Benedetti, Luke Ian
Preece, Robin
Papadopoulos, Panagiotis

Publication Date
2026-09-10

DOI
None/powerup_proceedings.69152

Bifurcation Analysis of Sub-Synchronous Oscillations Related to Grid-Forming Converter Inner Controllers

Luke Ian Benedetti, Robin Preece, Panagiotis N. Papadopoulos

University of Manchester

Suggested Citation

L. I. Benedetti, R. Preece, and P. N. Papadopoulos, "Bifurcation Analysis of Sub-Synchronous Oscillations Related to Grid-Forming Converter Inner Controllers," in *Proceedings of the PowerUp Conference*, 2026.

BibTeX Entry

```
@inproceedings{benedetti2026bifurcationanalysis,
  author = {Benedetti, Luke Ian and Preece, Robin and Papadopoulos, Panagiotis N.},
  title = {Bifurcation Analysis of Sub-Synchronous Oscillations Related to Grid-
      Forming Converter Inner Controllers},
  booktitle = {Proceedings of the PowerUp Conference},
  year = {2026},
}
```

Bifurcation Analysis of Sub-Synchronous Oscillations Related to Grid-Forming Converter Inner Controllers

Luke Ian Benedetti†, Robin Preece†, Panagiotis N. Papadopoulos†

***Abstract*—To ensure power system stability and security, it is vital to understand the complex nonlinear power system dynamics related to converter-interfaced generators. For example, grid-forming (GFM) converters are expected to be a key asset for maintaining a strong and stable power system, but might cause wide-bandwidth stability issues with underlying mechanisms heretofore unseen or understudied, including sub-synchronous oscillations (SSOs). This paper details a continuation-based bifurcation analysis of a GFM converter, revealing stability bounds with respect to operational conditions in addition to the time constant of the cascaded inner voltage and current controllers. We focus our analysis on the strong grid instability caused by an inner controller-related SSO, including continuation of the limit cycle past the Hopf bifurcation point, revealing rapid onset of unacceptably large oscillations. Furthermore, we investigate the impact of the circular current limiter, revealing spurious Hopf bifurcations in weak grids associated with the aforementioned SSO when adopting smooth approximations; this suggests the need for careful implementation of such approximations for GFMs, at least in bifurcation studies.**

***Index Terms*—Bifurcation, dynamics, grid-forming, limit cycle, nonlinear, sub-synchronous oscillation.**

I. Introduction

Grid-forming (GFM) devices are required for the formation and regulation of the voltage-sourced power system [1]. As such, GFM converters are expected to play a major role in the energy generation mixture [2] as fossil-fuelled synchronous generators are increasingly disconnected to meet critical decarbonisation goals [3]. Such technologies bring novel, wide-band dynamics spanning large frequency ranges [4] whose characteristics need to be fully understood to ensure desirable dynamic responses, avoid adverse interactions, oscillations, or instability, and design methods for the monitoring and mitigation thereof. Furthermore, single operating point small-signal analyses rely on localised linear assumptions, meaning they cannot capture important nonlinear dynamical phenomena including bifurcations and limit cycles [5]–[7]. As such, this paper performs a continuation-based bifurcation analysis of a standard GFM converter with cascaded control structure, revealing the nonlinear effects of operating conditions and inner controller time constants.

The standard cascaded GFM control structure [8] has known limitations with respect to inner controller tuning and strong grid instabilities [9]. In particular, the control system incites sub-synchronous oscillations (SSOs) related to the cascaded inner voltage and current controllers, seen to be around 12.5 Hz in [10], and 15 Hz to 17 Hz in [11]. Using a simplified model which allowed for analytical expression of the damping ratio of the SSO, the authors of [10] reveal the potential destabilising effect of increasing the current controller time constant or the filter capacitance, or decreasing the inner voltage controller proportional gain. Under different parametric conditions but with similar controller architecture, [12] finds slower strong grid instability-inducing SSOs of around 2.5 Hz which are related to interactions between the inner voltage and the outer synchronisation controllers. Meanwhile, [13] suggests increasing the voltage controller bandwidth to mitigate such issues. Whereas, in this paper we focus on the cascaded inner controller-related SSO, and investigate for the first time the parametric stability bounds of the (full detail) GFM converter with respect to codimension (codim)-2 continuation of the strong grid Hopf point of the SSO considering the time constants (bandwidths) of the inner voltage and current controllers simultaneously. We also consider stability bounds across a range of operational parameter variations with respect to the short-circuit ratio (SCR), X/R ratio, and active power set-point of the GFM.

Going beyond local equilibrium point bifurcation analysis, continuation of the limit cycle of a Hopf bifurcation has been seen to offer insights into the large-disturbance stability of a converter-based system [14], [15]. For example, we might observe a small region of attraction (RoA), caused by the unstable limit cycle that converges towards the stable equilibrium point prior to a subcritical Hopf bifurcation [14], [15]. Additionally, following a supercritical Hopf bifurcation, a stable limit cycle appears around the unstable equilibrium point [14], [16]. If said limit cycle is very small in magnitude then the system states (or observables) may stay well within the acceptable bounds, meaning by the formal power system stability definition [17] the system is stable, despite the local equilibrium point analysis suggesting instability. Both of these scenarios are ruled out for the GFM system in this work as we use normal form theory and limit cycle continuation to reveal that the strong grid Hopf point is supercritical with the emerging limit cycle quickly increasing to unacceptable levels.

Since continuation analysis typically requires a continuously differentiable vector field [6], [7], non-smooth elements such as saturation limiters require smooth approximations to be included in the analysis [18]. Therefore, we investigate the influence of including corresponding smooth approximations on the results of our bifurcation analyses. We find that smooth approximations of the circular current limiter can cause spurious Hopf bifurcations of the aforementioned SSO. This can invalidate the resultant bifurcation studies.

Ultimately, we add to the growing literature pertaining to

†All authors are with the Department of Electrical and Electronic Engineering, The University of Manchester, Manchester, UK. Emails: {luke.benedetti; robin.preece; panagiotis.papadopoulos}@manchester.ac.uk

Financial support is acknowledged from a UKRI Future Leaders Fellowship MR/Y00390X/1 (P. N. Papadopoulos and L. I. Benedetti) and EPSRC-funded Supergen Energy Networks Hub Project EP/S00078X/2 (R. Preece). All results can be fully reproduced using the methods and data described in this paper and provided references.

nonlinear dynamics, bifurcations and SSOs of GFM converters with a systematic, continuation-based bifurcation analysis of the standard cascaded control structure and concomitant SSOs. The contributions of this work include:

- Revealing stability bounds of GFM converters for key operational and control parameters via local bifurcation analysis. In particular, to the best of our knowledge, this has not previously been performed for the simultaneous tuning of the inner controller time constants.
- Unveiling the strong grid Hopf bifurcation of the inner controller-related SSO of the GFM to be supercritical with rapid onset of an unacceptably large limit cycle.
- Investigation of the impact of the circular current limiter smooth approximation, revealing potential for spurious Hopf bifurcations of the aforementioned SSO.
- We provide the Julia scripts for: modelling the GFM converter with ModelingToolkit.jl [19]; continuation analysis with BifurcationKit.jl [20], including bespoke wrappers required to enable this functionality; and nonlinear dynamical simulations with DifferentialEquations.jl [21].

II. Methodology

The analysis methodology adopted in this work is based on local (equilibrium point) bifurcation analysis [5]. In particular, we utilise a standard predictor-corrector continuation approach [20], [22]. In addition to this, continuation of the limit cycle is performed based on the collocation method [7], [20].

In this work, we consider a nonlinear dynamical system representation in ordinary differential equation (ODE) form,

$$\dot{\boldsymbol{x}} = \boldsymbol{f}(\boldsymbol{x}, \boldsymbol{p}), \tag{1}$$

where $\boldsymbol{f} : \mathbb{R}^N \times \mathbb{R}^{N_p} \rightarrow \mathbb{R}^N$ denotes a sufficiently smooth vector field [6] with N dynamic states, $\boldsymbol{x}$, and N_p parameters, $\boldsymbol{p}$. The dot operator signifies differentiation w.r.t. time.

A. Bifurcation Theory

Local bifurcation theory deals with the continuous change of parameters, finding points at which the qualitative behaviour of the nonlinear dynamical system suddenly changes apropos the stability of the equilibrium point [6], [23] evaluated at

$$0 = \boldsymbol{f}(\boldsymbol{x}, \boldsymbol{p}). \tag{2}$$

Such a change is reflected in the eigenvalues of the Jacobian of $\boldsymbol{f}(\boldsymbol{x})$ (i.e., evaluated at $\boldsymbol{p}$), often termed the state matrix $\boldsymbol{A}$, crossing into the right half-plane. With respect to codim-1 parameter variations [6], a single real-valued eigenvalue crossing results in aperiodic instability [24] and might indicate a pitchfork, transcritical, or saddle node bifurcation. However, the latter of these is more typical in power system scenarios in the form of voltage instability (e.g., maximum loadability limits), which from the nonlinear dynamical analysis perspective represents the point at which a stable and unstable equilibrium point collide and subsequently vanish [6] [25].

A pair of complex conjugate eigenvalues of $\boldsymbol{A}$ crossing the imaginary axis indicates a Hopf bifurcation, leading to oscillatory instability. A non-degenerate Hopf bifurcation [6] can be either supercritical or subcritical. For the former, a stable limit cycle emerges around the (now unstable) equilibrium point. The latter means an unstable limit cycle has collapsed onto the stable equilibrium point and the limit cycle disappears while the equilibrium point becomes oscillatory unstable (but without a nearby stable limit cycle as in the supercritical case).

Although not encompassed within the theory of bifurcations of continuously differentiable ODEs, the limit-induced bifurcation is an important consideration in modern power systems [26]. When a saturation limiter engages, the system undergoes a non-smooth change of its vector field. This essentially blocks the controllers "behind" the saturation limiter thereby eliminating the corresponding equations and dynamic states. [26] highlights that such a change of the governing equations can immediately shift the system to an unstable state. However, non-smooth action is not compatible with standard continuation methods [6], thereby incentivising the use of smooth approximations for non-smooth elements [18]. The smooth approximation used in this work is discussed in more detail in Section III-D.

B. Continuation of Equilibrium Branch or Bifurcation Branch

Starting from a known initial condition, continuation methods follow the equilibrium branch, along which (2) holds true, as a parameter is varied. Fundamentally, this involves a predictor and a corrector step [7], with one of the most common and robust algorithms being pseudo-arclength continuation (PALC) as implemented in this work using BifurcationKit.jl (BFK) [20]. Bifurcation points are identified based on the behaviour of the eigenvalues of the Jacobian as discussed in Section II-A.

Once a bifurcation point is identified, a second continuation parameter can be selected and they can be varied simultaneously along the bifurcation curve for which the relevant eigenvalue(s) remain on the imaginary axis. If no other bifurcation branches are found within the (codim-2) parameter space considered, this bifurcation branch represents the stability boundary. This procedure is performed for the strong grid Hopf bifurcation in this work.

C. Hopf Normal Form and Limit Cycle Continuation

In this work, we find that the strong grid Hopf bifurcation is supercritical, meaning that a limit cycle emerges after the Hopf point. This is determined by considering the centre manifold theorem [6] which states that the dynamics of the system can be reduced to a two-dimensional invariant manifold[1] near the Hopf bifurcation point. The normal form of the Hopf bifurcation can be calculated by considering the third-order Taylor series approximation of the centre manifold, which captures the nonlinear effects that determine whether the Hopf bifurcation is subcritical, supercritical, or degenerate (Section II-A). In particular, the Hopf normal form as considered in BFK is

$$\dot{\boldsymbol{z}} = \boldsymbol{z}\left(j\omega + a\,\delta p + b\,|\boldsymbol{z}|^2\right), \tag{3}$$

[1]This is the centre manifold. It can be noted that, at the bifurcation point, it is tangent to the plane spanned by the corresponding eigenvectors [6].

where $\boldsymbol{z}$ is a complex phasor, ω is the frequency of the complex conjugate eigenvalue pair giving rise to the Hopf bifurcation, a quantifies the linear growth of the limit cycle, which holds true for very small values of the change in continuation parameter [6], δp. The first Lyapunov coefficient is given by b, whose real part indicates supercriticality if negative, subcriticality if positive, and degeneracy if zero.

We can then apply continuation to the limit cycle itself[2] as the parameter continues to change. This requires an estimation of the limit cycle, as represented as a boundary value problem, achieved in this case using the orthogonal collocation method [27], again implemented with BFK [20]. Therefore, as we further change the continuation parameter, we can track the period and envelope of the limit cycle. In our (supercritical) case, this is done to check whether the resulting oscillation remains small or quickly increases to unacceptably large values (e.g., extensive voltage and current swings).

III. Grid-Forming Converter System Under Test

All models were implemented in the Julia programming language using ModelingToolkit.jl (MTK) within the SciML ecosystem[3] [19]. The nominal parameters are displayed in Table I and described further throughout this section. The * superscript denotes references and set points.

TABLE I: Nominal Parameters of the GFM-Infinite Bus System

Parameter	Value	Parameter	Value
P^*	0.8 pu	m_p	0.01 pu
Q^*	0 pu	$\omega_{c,p}$	$2\pi 5$ rad s^{-1}
V^*	1 pu	m_q	0.01 pu
ω_b	$2\pi 50$ rad s^{-1}	$\omega_{c,q}$	$2\pi 5$ rad s^{-1}
R_f	0.03 pu	ζ_{IVC}	0.7
$X_{l,f}$	0.08 pu	τ_{IVC}	45 ms
$X_{c,f}$	13.51 pu	ζ_{ICC}	0.7
SCR	2.5	τ_{ICC}	1.5 ms
X/R	10	$\lvert\boldsymbol{i}\rvert_{\max}$	1.2 pu
		T_s	47.12 ms

The models of the electrical and GFM control systems are completed in independent rotating reference frames, synchronised to the grid voltage angle, $\angle \boldsymbol{v_g}$, and virtual rotor speed, θ, respectively. A phasor can then be denoted in the form $\boldsymbol{\nu} = \nu_d + j\nu_q$ and physical signals in the control frame are discerned by superscript ^{ctrl}. Conversion of signals between reference frames is through a geometric transform [18].

A. Electrical System

We consider a GFM voltage-sourced converter (VSC) connected to a Thévenin equivalent grid model. The single line circuit diagram is illustrated in Fig. 1, where $\boldsymbol{v_{cv}}$, $\boldsymbol{v_m}$, and $\boldsymbol{v_g}$ are the voltages at the converter switches, across the filter capacitor, and of the Thévenin equivalent infinite bus,

[2]A detailed technical discussion of this is out of the scope of this paper and the reader is referred to [6], [20] for more information.

[3]The corresponding modelling (and analysis) scripts are available in [28]. Note, bespoke wrappers for extraction of the vector field and Jacobians of a hierarchically constructed MTK model are provided to allow for continuation analysis with the BifurcationKit.jl package [20].

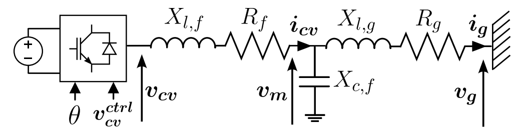

Fig. 1: Single line circuit diagram of grid-forming converter connected to Thévenin equivalent grid model.

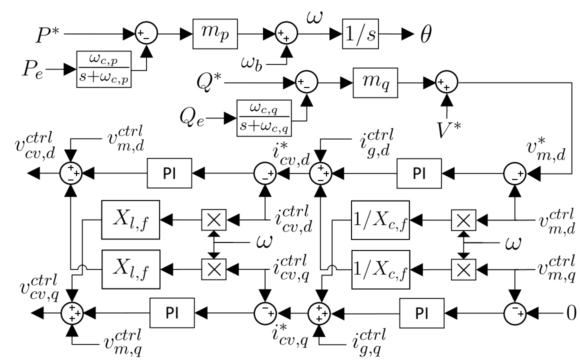

Fig. 2: Multi-loop, droop-based GFM controller.

respectively. The current through the coupling filter and grid impedance are denoted by $\boldsymbol{i_{cv}}$ and $\boldsymbol{i_g}$, respectively. The VSC is the averaged model with θ and $\boldsymbol{v_{cv}^{ctrl}}$ denoting the virtual rotor angle of the GFM and the requested value of $\boldsymbol{v_{cv}}$ in the controller reference frame, respectively. Furthermore, we consider that, on the timescales of interest, there is sufficient power available from the primary source to compensate for any current drawn, thereby allowing representation with an ideal voltage source on the DC side of the converter.

The per unit resistance, inductive reactance, and capacitive reactance of the coupling filter are denoted by R_f, $X_{l,f}$, and $X_{c,f}$, respectively. The resistance and inductive reactance of the Thévenin equivalent grid are R_g and $X_{l,g}$ but when it comes to continuation, we are more interested in these parameters from the perspective of the short circuit ratio (SCR) and the X/R ratio, with the corresponding conversion

$$SCR = 1/\sqrt{\left(R_g^2 + X_{l,g}^2\right)}, \tag{4}$$

$$X/R = X_{l,g}/R_g. \tag{5}$$

B. Droop Control

The full GFM control system block diagram is illustrated in Fig. 2. The active power/synchronisation controller is a standard droop with low-pass filter. The droop gain and cut-off frequency are denoted by m_p and $\omega_{c,p}$, respectively. Also included is a reactive power droop which augments the voltage magnitude reference with droop gain and cut-off frequency denoted by m_q and $\omega_{c,q}$, respectively.

C. Inner Voltage and Current Controllers

The inner voltage and current controllers adopt a vector control architecture including proportional-integral (PI) regulators in addition to feed-forward and decoupling terms [8]. The proportional and integral gains are denoted by $K_{p,IVC}$ and $K_{i,IVC}$, and $K_{p,ICC}$ and $K_{i,ICC}$ for the inner voltage and current PI controllers, respectively. Tuning of the inner controllers is achieved independently using pole-placement.

For the inner current controller, assuming ideal timescale separation, neglection of pulse-width modulation (PWM)/control delay, and considering identical d-axis and q-axis control loops [29], the closed loop consists of the transfer functions of the PI controller,

$$G_{PI}(s) = K_{p,ICC} + \frac{K_{i,ICC}}{s}, \tag{6}$$

and the RL branch of the output filter,

$$G_{RL}(s) = \frac{1}{(X_{l,f}/\omega_b)s + R_f}, \tag{7}$$

with unity feedback of the measured output current, $\boldsymbol{i_{cv}}$. The resulting characteristic equation is

$$s^2 + \frac{R_f + K_{p,ICC}}{(X_{l,f}/\omega_b)}s + \frac{K_{i,ICC}}{(X_{l,f}/\omega_b)} = 0. \tag{8}$$

We can then compare this to the standard second-order characteristic equation with natural frequency of $\omega_{n,ICC}$ and damping ratio of ζ_{ICC}, giving PI controller gains in the form

$$K_{p,ICC} = 2\,\zeta_{ICC}\,\omega_{n,ICC}\,\frac{X_{l,f}}{\omega_b} - R_f, \tag{9}$$

$$K_{i,ICC} = \omega_{n,ICC}^2\frac{X_{l,f}}{\omega_b}. \tag{10}$$

The speed of the closed-loop response can then be chosen by considering the relation between $\omega_{n,ICC}$, ζ_{ICC} and the 5% settling time, termed τ_{ICC} for the inner current controller, based on the approximate relation

$$\tau_{ICC} \approx \frac{3}{\zeta_{ICC}\,\omega_{n,ICC}}. \tag{11}$$

Rearranging (11) for $\omega_{n,ICC}$ and substituting back into (9) and (10) allows us to tune our closed-loop response based only on ζ_{ICC} (which we keep constant at 0.7) and τ_{ICC}, which is used for the continuation analysis.

We perform a similar procedure for the inner voltage controller, resulting in PI controller gains of

$$K_{p,IVC} = \frac{6}{\tau_{IVC}\,\omega_b\,X_{c,f}}, \tag{12}$$

$$K_{i,IVC} = \frac{9}{\zeta_{IVC}^2\,\tau_{IVC}^2\,\omega_b\,X_{c,f}}. \tag{13}$$

D. Current Limitation

To protect the converter switches from over-current conditions, a circular current limiter can be included [30]. This is described as

$$\boldsymbol{i^*_{lim}} = \rho \times \boldsymbol{i^*}, \tag{14}$$

$$\rho = \min(1, |\boldsymbol{i}|_{\max}/|\boldsymbol{i^*}|), \tag{15}$$

where $\boldsymbol{i^*}$, $\boldsymbol{i^*_{lim}}$, $|\boldsymbol{i}|_{\max}$ are the unsaturated and saturated current references, and the maximum current magnitude, respectively. It is also standard practice to include anti-windup control in this scenario to avoid accumulation of the integral output for the inner voltage PI controllers when the current reference is saturated. In particular, we adopt the common back-calculation and tracking method as per [31]. This approach requires the tuning of a tracking time constant, T_s, for which there exists several different recommendations. We adopt the suggestion from [31] where $T_s = K_{i,IVC}$.

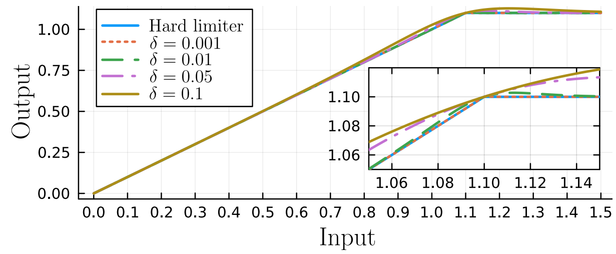

Fig. 3: Input-output (unsaturated-saturated current reference in per unit) response of current limiter with different values of the smoothing parameter δ. The inset zooms on the knee point.

As discussed in Section II-A, we investigate the impact of a smooth approximation of the current limiter, as is required for inclusion within continuation analysis [18]. In particular, we consider the transition from non-limited to limited conditions (and vice versa) as a Heaviside step function approximated based on the hyperbolic tangent function [18] as

$$\boldsymbol{i^*_{lim}} = (1-\alpha) \times \boldsymbol{i^*} + \alpha \times |\boldsymbol{i}|_{\max} e^{j\angle \boldsymbol{i^*}} \tag{16}$$

with

$$\alpha = \frac{1}{2}\left(1 + \tanh\left(\frac{|\boldsymbol{i^*}| - |\boldsymbol{i}|_{\max}}{2\times\delta}\right)\right) \tag{17}$$

where δ is a "smoothing" parameter, the impact of which is illustrated in Fig. 3. Particularly, δ of 0.001 and 0.01 provide very close approximations to the ideal (hard) response, while more noticeable, but not ostensibly significant, divergence is seen for δ of 0.05 and 0.1. Please see Appendix A for time-domain validation of the system response when adopting the current limiter smooth approximation.

IV. Bifurcation Analysis and Results

In this section, parametric stability bounds are illustrated based on continuation analysis of operational parameters and inner controller time constants. Additionally, we continue the limit cycle associated with the strong grid Hopf bifurcation to reveal rapid onset of unacceptably large oscillations. Finally, we study the impact of the circular current limiter smooth approximation to show the existence of spurious Hopf bifurcations that can invalidate corresponding analyses.

A. Continuation of Operational Parameters

Beginning with the nominal parameters outlined in Table I (current limitation not yet included), we choose the SCR as continuation parameter, and display the equilibrium branch results for differing values of active power set point, P^*, in Fig. 4. Bifurcations are found to occur in both weak grid ($SCR \lesssim 1$) and strong grid scenarios ($SCR \approx 4.95$). The former is the saddle node bifurcation due to the maximum power transfer limits [25] in a lossy system as per [32]

$$P_{\max} = \frac{|\boldsymbol{v_m}|}{R_g^2 + X_g^2}\left(|\boldsymbol{v_m}|\,R_g + |\boldsymbol{v_g}|\sqrt{R_g^2 + X_g^2}\right), \tag{18}$$

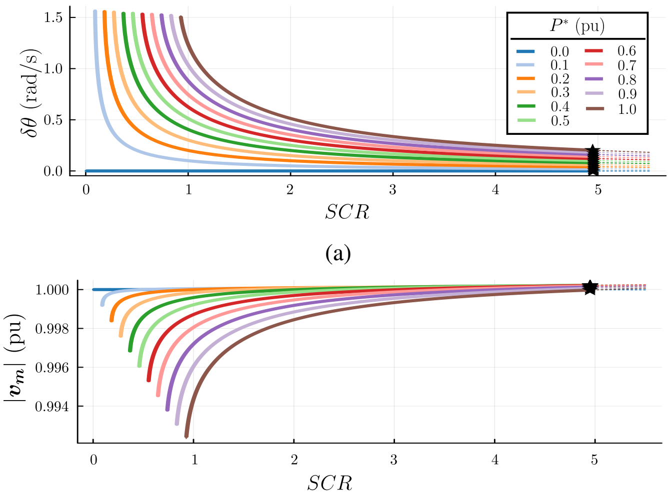

(a)

(b)

Fig. 4: Bifurcation diagram for (a) $|\boldsymbol{v_m}|$ and (b) $\delta\theta$ for varying SCR, with different values of P^*. A star shows the Hopf point and thin dotted line shows unstable points.

and with $X_g = 10R_g$, $P_{\max}$ occurs at $\delta\theta \approx \angle \boldsymbol{v_m} - \angle \boldsymbol{v_g} = \pi/2 + \tan^{-1}(R_g/X_g)$ rad $= 1.6705$ rad. In this case, as observed in Fig. 4a, the continuation algorithm fails[4] as we approach the saddle node ($P_{\max}$) point. To confirm this behaviour, we can observe the real part of the rightmost (real-valued) eigenvalue as we approach the weak grid instability point in Fig. 5 (for $P^* = 0.8$ pu), where we find that a single real-valued eigenvalue approaches the stability boundary before the continuation corrector step fails to converge. Particularly, for a given X/R ratio, R_g and X_g will increase as SCR decreases due to (4). Therefore, especially for relatively small variations of $|\boldsymbol{v_m}|$ (Fig. 4b), $P_{\max}$ reduces, and once $P_{\max}$ becomes less than P^*, the equilibrium point vanishes.

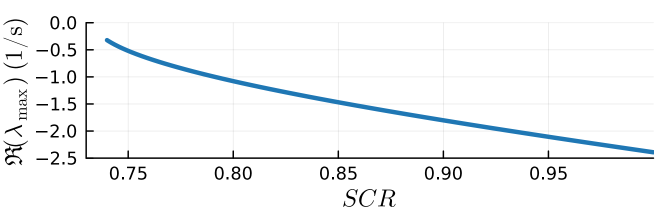

Fig. 5: Trajectory of the real part of the rightmost eigenvalue, $\Re(\lambda_{\max})$, as the SCR is varied, with $P^* = 0.8$ pu.

The strong grid instability is related to the Hopf bifurcation associated with the inner controller-related SSO[5], and is seen to be largely unaffected by P^*. Considering converter-interfaced generators may be connected at different voltage levels, with different X/R ratios, we also perform codim-2 continuation (Section II-B) of this strong grid Hopf point, varying the X/R ratio along with the SCR. This is displayed in Fig. 6, with the colourbar relaying the frequency of the SSO along the Hopf branch. We find that decreasing the X/R ratio increases the SCR at which the strong grid instability occurs, suggesting that distribution-connected GFMs utilising the prototypical control scheme of Fig. 2 can be connected in stronger grids than transmission system-connected GFMs. We can also note that the frequency of the corresponding SSO reduces with the reduction of X/R ratio (and concomitant increase of SCR). At the nominal $X/R = 10$, the frequency is 25.58 Hz, whereas this reduces to 5.71 Hz at $X/R = 0.1$.

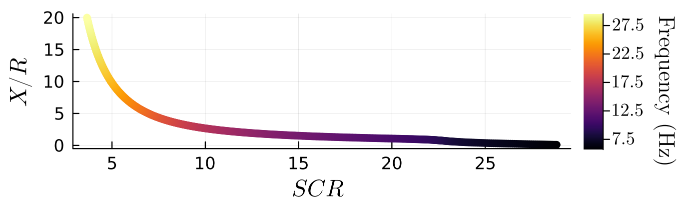

Fig. 6: Bifurcation diagram for simultaneous variation of SCR and X/R ratio, following the strong grid Hopf bifurcation.

B. Continuation of the Limit Cycle

Returning to the nominal parameters of $X/R = 10$ and $P^* = 0.8$ pu, we can apply the normal form analysis (Section II-C) to the strong grid Hopf bifurcation. We find that the first Lyapunov coefficient, denoted as b in (3), is equal to $-0.00198 - j0.00096$. Since the real part of b is negative, the Hopf bifurcation is supercritical[6] and a stable limit cycle emerges as the parameter continues past the bifurcation point.

We can then perform continuation of the limit cycle (Section II-C) and observe the impact on $|\boldsymbol{v_m}|$ and $|\boldsymbol{i_{cv}}|$. The corresponding maximum and minimum of the magnitude of the limit cycle are displayed in Fig. 7, revealing that very small increase of the SCR past the bifurcation point results in rapid growth of the limit cycle, quickly reaching unacceptable levels. Note, $|\boldsymbol{i_{cv}}|$ constitutes a magnitude which is why the lower bound of the limit cycle appears to "bounce" off of zero, when it is rather changing direction.

C. Continuation of Inner Controller Time Constants

As previously discussed, the strong grid instability-inducing SSO results from an interaction involving the cascaded inner voltage and current controllers [10], [11]. Therefore, in this subsection we perform codim-2 continuation analysis of the Hopf bifurcation with respect to the inner controller time constants τ_{IVC} and τ_{ICC} (Section III-C). The continuation plot, with the nominal parameters of Table I, is displayed in in Fig. 8. Clearly, the parametric stability bounds indicate

[4]Continuation algorithms can fail near the saddle-node point, especially in stiff systems such as the one being studied. This is because the Jacobian becomes increasingly ill-conditioned near the critical point [33], causing the predictor step to provide poor estimates to the corrector, whose own convergence also degrades due to the ill-conditioning. In this case, extremely small steps of the bifurcation parameter are required to improve the likelihood of Newton convergence, eventually hitting minimum thresholds and computational limits. Furthermore, the fold, as seen in Fig. 4, is very sudden with the voltage magnitude and angle nearing vertical at the failure point.

[5]The inner controller characteristics of these SSOs are discussed in [10] and [11] and, although not displayed for brevity, confirmed in this work through participation factor analysis.

[6]The supercriticality of the Hopf bifurcation is consistent across the different parameter conditions analysed in this work, except when adopting the smooth current limiter approximation, as per Appendix B.

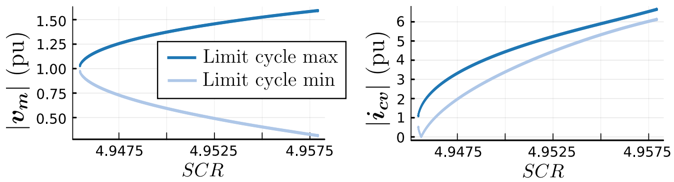

(a) (b)

Fig. 7: Bifurcation diagram showing the maximum and minimum bounds of the limit cycle as SCR is continued past the strong grid Hopf bifurcation point.

that the time constants for the inner voltage and current controllers must be sufficiently large and small, respectively, highlighting the need for sufficient timescale separation in strong grid-connected GFM control designs. Consequently, if the bandwidth of the inner current controller is limited due to reduced switching frequency of the converter, the inner voltage controller must be sufficiently slow to maintain stability. However, if $\tau_{ICC} \gtrapprox 2.5$ ms when $SCR = 5$, then tuning τ_{IVC} cannot bring stability in strong grids.

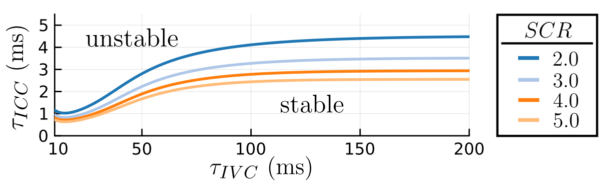

Fig. 8: Bifurcation diagram for simultaneous variation of τ_{IVC} and τ_{ICC} ratio, following the strong grid Hopf bifurcation.

D. Impact of Current Limiter Smooth Approximation

In this subsection, we re-perform the SCR continuation analysis from Section IV-A but with the addition of the circular current limiter outlined in Section III-D. We consider both the ideal (hard) limiter and the ostensibly very good smooth approximations of $\delta = 0.001$ and $\delta = 0.01$, with $P^* = 1$ pu. The continuation results for the smooth approximations are displayed in Fig. 9, while the hard limiter continuation gives the same curve shape as the $\delta = 0.001$ but without the Hopf points (included in Appendix B for completeness), and it fails at the limit-induced bifurcation point. In particular, this spurious Hopf bifurcation occurs in the weak grid scenario when SCR is reduced to 1.043 and 1.234 for $\delta = 0.001$ and $\delta = 0.01$ respectively, despite not occurring when the ideal (hard) limiter is modelled. The corresponding complex conjugate pair of eigenvalues then returns to stability just before the limit-induced bifurcation point [26] (at $I_{cv} = 1.1$ pu and $SCR \approx 1.033$) when $SCR = 1.034$ and $SCR = 1.048$ for $\delta = 0.001$ and $\delta = 0.01$ respectively. Furthermore, analysing the corresponding eigenvalue trajectory in Fig. 10 reveals that this Hopf bifurcation is induced by the same SSO that causes the strong grid Hopf bifurcation. It can also be noted that the strong grid Hopf bifurcation appears at a lower value of $SCR = 4.390$ when $\delta = 0.01$.

Further analysis of this spurious Hopf bifurcation can be found in Appendix B, also revealing that the smooth approximation can change the strong grid (and corresponding weak grid) Hopf to subcritical. However, this ultimately constitutes a modelling artefact (i.e., it is not present when using the hard limiter model) that can invalidate the results of bifurcation analysis, suggesting false instabilities. Subsequently, extreme caution, and careful validation is recommended if adopting smooth current limiter approximations.

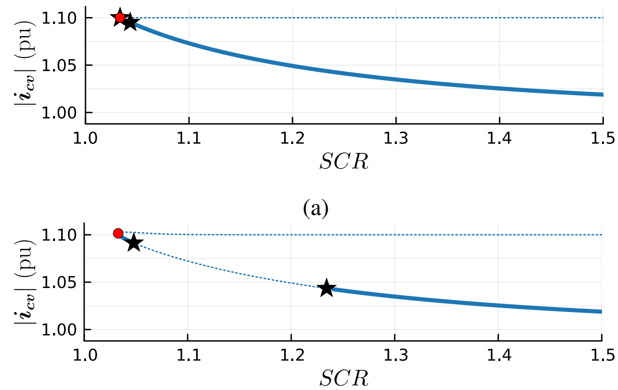

(a)

(b)

Fig. 9: Bifurcation diagram of $|\boldsymbol{i_{cv}}|$ against SCR with smooth limiter with (a) $\delta = 0.001$ and (b) $\delta = 0.01$. Black stars and red circles show Hopf and limit-induced bifurcation points, respectively. Thin dotted lines denote instability.

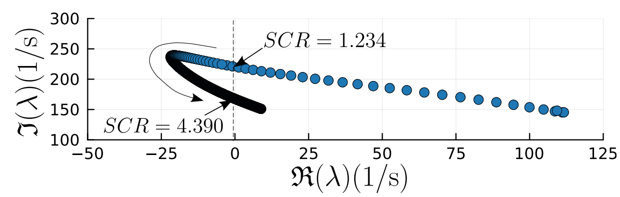

Fig. 10: Trajectory of the strong grid instability-inducing SSO eigenvalue, λ, as SCR varies between 1.075 and 5.5 with circular current limiter smooth approximation with $\delta = 0.01$.

V. Conclusions

This paper details a continuation-based bifurcation analysis of a grid-tied multi-loop controlled GFM converter. In particular, focus is given to an inner controller-related SSO that can incite instability in strong grids. Parametric stability bounds are outlined for a range of SCR, X/R ratio, and active power set point conditions, as well as highlighting the need for sufficiently small and large time constants for the inner current and voltage controllers, respectively.

Additionally, we reveal through normal form theory that the corresponding Hopf bifurcation is supercritical, and find that subsequent continuation of the bifurcation parameter leads to rapid onset of unacceptably large limit cycle oscillations (e.g., extensive voltage and current swings).

Finally, we find that the adoption of smooth approximations of the (circular) current limiter can cause spurious Hopf bifurcations of the aforementioned SSO in weak(er) grid conditions, representing a modelling artefact, even for ostensibly sufficient approximations of the ideal saturation response.

APPENDIX

A. Time-Domain Validation of the Circular Current Limiter Smooth Approximation

To add to the static input-output visualisation of Fig. 3, we consider here the time-domain response of the system under test in response to a grid voltage magnitude dip from 1 pu to 0.9 pu which starts at 0.01 s and lasts 20 ms. Parameters are set to nominal values of Table I but with $P^* = 1$ pu. It can be seen from Fig. 11 that $\delta = 0.001$ provides a very good approximation to the ideal hard current limiter response, while $\delta = 0.01$ results in some slight but not significant discrepancies. When adopting δ of 0.05 or 0.1, the time-domain response shows instability, the reason for which can be understood based on the spurious Hopf bifurcations as discussed in Section IV-D and Appendix B.

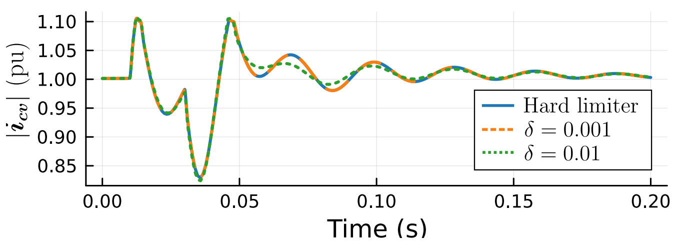

Fig. 11: Time-domain response of $|\boldsymbol{i_{cv}}|$ when the system is subject to a grid voltage dip, when including current limiter with ideal (hard) response as well as smooth approximation with $\delta = 0.001$ and $\delta = 0.01$.

B. Supplementary Analysis of the Spurious Hopf Bifurcation

For completeness, Fig. 12 displays the SCR continuation with hard limiter model, for comparison against Fig. 9. This confirms the lack of weak grid Hopf bifurcation, and the failure of the continuation at the limit-induced bifurcation point (i.e., no subsequent thin dotted line as in the smooth approximation case).

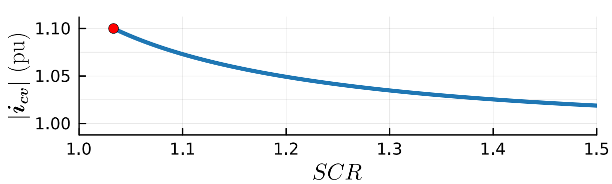

Fig. 12: Bifurcation diagram of $|\boldsymbol{i_{cv}}|$ against SCR with hard current limiter model. The red circle shows the limit-induced bifurcation point.

We can continue the (spurious) weak grid Hopf point by varying the smoothing parameter δ along with the SCR as per Fig. 13. This reveals that further increase of δ increases (worsens) the lower SCR stability boundary associated with this Hopf bifurcation. At the same time, we observe that the weak and strong grid Hopf bifurcations approach each other as δ is increased, until they meet at $\delta = 0.0142$ and any further increase results in instability at all points for the range of SCR considered. This behaviour can be intuitively (yet crudely) understood by considering the whole eigenvalue curve of Fig. 10 moving to the right as we increase δ.

It can also be noted that the strong grid Hopf bifurcation remains supercritical only for very small values of δ with a Bautin (generalized Hopf) bifurcation occurring when $\delta \approx 0.0011$ and $SCR \approx 4.944$, after which (i.e., smaller SCR) the bifurcation is instead subcritical. The (spurious) weak grid Hopf bifurcation is always subcritical.

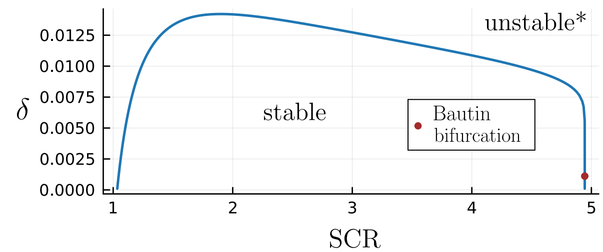

Fig. 13: Bifurcation diagram for simultaneous variation of SCR and δ, following the weak grid Hopf bifurcation (which is seen to lead into the strong grid Hopf) when adopting smooth approximation of the circular current limiter. Note, the SSO returning to stability (at $SCR = 1.043$) just before the limit-induced bifurcation point, as discussed in Section IV-D, means that the stability of the system is not solely delineated by the Hopf curve, hence the * superscript in the unstable label.

REFERENCES

[1] Y. Li, Y. Gu, and T. C. Green, "Revisiting grid-forming and grid-following inverters: A duality theory," *IEEE Transactions on Power Systems*, vol. 37, no. 6, pp. 4541–4554, 2022.

[2] B. Badrzadeh, C. Cardozo, M. Hishida, S. Shah, I. Huq, N. Modi, and A. Morton, "Grid-forming inverters: Project demonstrations and pilots," *IEEE Power and Energy Magazine*, vol. 22, no. 2, pp. 66–77, 2024.

[3] International Energy Agency (IEA), "Renewables 2024," Paris, October 2024, License: CC BY 4.0. [Online]. Available: https://www.iea.org/reports/renewables-2024

[4] J. Shair, H. Li, J. Hu, and X. Xie, "Power system stability issues, classifications and research prospects in the context of high-penetration of renewables and power electronics," *Renewable and Sustainable Energy Reviews*, vol. 145, p. 111111, 2021.

[5] S. H. Strogatz, *Nonlinear Dynamics and Chaos: With Applications to Physics, Biology, Chemistry, and Engineering*, 2nd ed. 600 Broken Sound Parkway NW, Suite 300, Boca Raton FL, 33487-2742: CRC Press, Taylor & Francis Group, 2018.

[6] Y. A. Kuznetsov, *Elements of Applied Bifurcation Theory*, 2nd ed., ser. Applied Mathematical Sciences. Springer-Verlag New York, Inc., 1998, vol. 112.

[7] G. Datseris and U. Parlitz, *Nonlinear Dynamics: A Concise Introduction Interlaced with Code*, 1st ed., ser. Undergraduate Lecture Notes in Physics. Springer Nature Switzerland AG, 2022.

[8] N. Baeckeland, D. Pal, G.-S. Seo, B. Johnson, and S. Dhople, "Large-signal stability analysis of grid-forming inverters with equivalent-circuit models," *IEEE Transactions on Energy Conversion (Early Access)*, pp. 1–13, 2025.

[9] M. S. Javaid, B. Chaudhuri, F. Teng, and Z. Akhtar, "A novel tuning method of grid-forming inverter voltage control," in *IEEE PowerTech 2025*, Kiel, Germany, 2025.

[10] ——, "Impact of inner control in GFM-induced sub-synchronous oscillations," in *2025 IEEE PES General Meeting*, Austin, TX, USA, 2025.

[11] L. I. Benedetti, P. N. Papadopoulos, and R. Preece, "Exploring the variation of critical modal properties in power systems with converter-interfaced units," *Sustainable Energy, Grids and Networks*, vol. 43, p. 101841, 2025.

[12] Z. Hong, H. Xu, Z. Hou, and M. Zhan, "Origin of anomalous instability of grid-forming converters tied to stiff grid," *IET Renewable Power Generation*, vol. 17, no. 10, pp. 2563–2574, 2023.

[13] X. Li, X. Xiong, C. Li, and Z. Zhou, "Analysis on instability mechanism of grid-connected VSG under strong grid condition," in *2024 IEEE 10th International Power Electronics and Motion Control Conference (IPEMC2024-ECCE Asia)*, 2024, pp. 2118–2121.

[14] X. Ma, Y. Wan, Y. Wang, X. Dong, S. Shi, J. Liang, Y. Zhao, and H. Mi, "Multi-parameter practical stability region analysis of wind power system based on limit cycle amplitude tracing," *IEEE Transactions on Energy Conversion*, vol. 38, no. 4, pp. 2571–2583, 2023.

[15] B. Zhao, Z. Huang, L. Chen, K. Hou, Y. Min, and S. Luo, "Limit cycle and large signal stability boundary induced by outer controller of grid-connected VSC," *IEEE Journal of Emerging and Selected Topics in Power Electronics (Early Access)*, 2025.

[16] M. S. Zazo and J. D. M. Rademacher, "Lyapunov coefficients for Hopf bifurcations in systems with piecewise smooth nonlinearity," *SIAM J. on Appl. Dyn. Syst.*, vol. 19, no. 4, pp. 2847–2886, 2020.

[17] N. Hatziargyriou, J. Milanovic, C. Rahmann, V. Ajjarapu, C. Canizares, I. Erlich, D. Hill, I. Hiskens, I. Kamwa, B. Pal, P. Pourbeik, J. Sanchez-Gasca, A. Stankovic, T. Van Cutsem, V. Vittal, and C. Vournas, "Definition and classification of power system stability – revisited & extended," *IEEE Trans. on Power Systems*, vol. 36, no. 4, pp. 3271–3281, 2021.

[18] D. Moutevelis, J. Roldán-Pérez, M. Prodanovic, and S. Sanchez-Acevedo, "Bifurcation analysis of active electrical distribution networks considering load tap changers and power converter capacity limits," *IEEE Trans. on Power Electronics*, vol. 37, no. 6, pp. 7230–7246, 2022.

[19] Y. Ma, S. Gowda, R. Anantharaman, C. Laughman, V. Shah, and C. Rackauckas, "Modelingtoolkit: A composable graph transformation system for equation-based modeling," *arXiv*, 2021, doi:10.48550/arXiv.2103.05244.

[20] R. Veltz, "BifurcationKit.jl," Jul. 2020. [Online]. Available: https://hal.archives-ouvertes.fr/hal-02902346

[21] C. Rackauckas and Q. Nie, "DifferentialEquations.jl–a performant and feature-rich ecosystem for solving differential equations in Julia," *Journal of Open Research Software*, vol. 5, no. 1, 2017.

[22] H. B. Keller, *Lectures on Numerical Methods in Bifurcation Problems - Tata Institute Lectures on Mathematics and Physics*. Springer Berlin Heidelberg, 1988.

[23] Y. Chen, R. Preece, and M. Barnes, "Identifying feasibility region boundaries in power systems with multiple VSCs," *IEEE Transactions on Power Systems*, vol. 38, no. 2, pp. 1229–1241, 2023.

[24] P. S. Kundur, *Power System Stability and Control*, 3rd ed. McGraw-Hill, 2017.

[25] T. van Cutsem and C. Vournas, *Voltage Stability of Electric Power Systems*. New York, NY, USA: Springer, 2007.

[26] G. Xing, Y. Min, L. Chen, and H. Mao, "Limit induced bifurcation of grid-connected VSC caused by current limit," *IEEE Transactions on Power Systems*, vol. 36, no. 3, pp. 2717–2720, 2021.

[27] E. J. Doedel, W. Govaerts, Y. A. Kuznetsov, and A. Dhooge, "Numerical continuation of branch points of equilibria and periodic orbits," *International Journal of Bifurcation and Chaos*, vol. 15, no. 03, pp. 841–860, 2005, doi:10.1142/S0218127405012491.

[28] L. I. Benedetti, R. Preece, and P. N. Papadopoulos, "Modelling and dynamic analysis of a grid-forming converter in Julia," Jun 2026, software, doi:10.48420/32802230.

[29] A. Yazdani and R. Iravani, *Voltage-Sourced Converters in Power Systems: Modeling, Control, and Applications*. Hoboken, New Jersey: John Wiley & Sons, Inc., 2010.

[30] N. Baeckeland, D. Chatterjee, M. Lu, B. Johnson, and G.-S. Seo, "Overcurrent limiting in grid-forming inverters: A comprehensive review and discussion," *IEEE Transactions on Power Electronics*, vol. 39, no. 11, pp. 14 493–14 517, 2024.

[31] A. Visioli, *Practical PID Control*. London, UK: Springer London, 2006.

[32] B. Pepper and D. Campos-Gaona, "Impedance estimation for transient stability enhancement of virtual synchronous machines," in *2024 IEEE 15th International Symposium on Power Electronics for Distributed Generation Systems (PEDG)*, 2024, pp. 1–6.

[33] V. Ajjarapu and C. Christy, "The continuation power flow: a tool for steady state voltage stability analysis," *IEEE Transactions on Power Systems*, vol. 7, no. 1, pp. 416–423, 1992.

I. Review #39A

A. Paper summary

Understanding the complex, nonlinear dynamics of grid-forming (GFM) converters is essential for grid stability because these devices can trigger unique, wide-bandwidth oscillations, such as sub-synchronous oscillations (SSOs). This paper uses bifurcation analysis to identify stability thresholds related to controller configurations and current limiters. The paper emphasizes the impact of modeling artifacts and demonstrates how inner-loop controllers and specific smoothing approximations can cause abrupt, widespread instability.

B. Comments for authors

This paper provides a compelling assessment of grid-forming (GFM) converter nonlinear dynamics through bifurcation analysis, Hopf normal forms, limit cycle continuation, and the center manifold theorem. It is an excellent contribution. These classical tools effectively extend analysis beyond small-signal stability at a single equilibrium. Furthermore, this work demonstrates to the power systems community that nonlinear dynamics can be assessed via formal, tractable approaches—at least for a Single Machine Infinite Bus (SMIB) case—rather than relying solely on time-domain sensitivity analysis.

Some comments:

- The true current-limiting strategy should be recalled in the paper. As far as I understand it $i^*_{lim} = \rho \cdot i^*$, where $\rho = \min(1, \frac{|i|_{max}}{|i^*|})$.
- It would be interesting to analyze other current-limiting strategies and their smooth approximations. Examples include nonlinear/adaptive virtual impedance, noncircular limiters (d or q priorities), threshold-based switching (GFM -¿ GFL), direct voltage magnitude and phase limiting, etc. Some of these strategies may exhibit similar behavior to the one you showed due to modeling artifacts.
- The SMIB test case is certainly a mandatory step when analyzing the nonlinear dynamics of grid-forming (GFM) converters. An even more interesting extension of the analysis would be to include a small triangular test case: two GFM converters connected together and to an infinite bus. Is this extension feasible? As far as I know, defining a common rotating framework for grid equations is an open question in large disturbance analysis. A brief discussion of this critical issue at the end of the paper would be valuable for future work.

C. Summarize your recommendation in one to two sentences

Analyzing other current-limiting strategies would be valuable. Some strategies may exhibit behavior similar to what you demonstrated due to modeling artifacts.

Discussing possible extensions for analyzing multi-grid forming converters would be interesting and could define future work on this topic. This could be added to the Notes Papers section.

— Anonymous reviewer

II. Review #39B

A. Paper summary

The paper conduct bifurcation analysis of a grid forming converter (BFM). The focus is the study of stability or oscillatory behavior as the short circuit ratio (SCR, the reciprocal of the Thevenin equivalent f grid impedance) or inner controller time constants change, for both strong (high SCR) and weak (low SCR) grid, for different values of active power set points and X/R ratios of the gird Thevenin equivalent. It also studies the effect of smooth approximations of (nonsmooth) current limits and finds that it can give rise to spurious strong grid Hopf bifurcations. Simulation results of these scenarios are presented to illustrate the main conclusions.

B. Comments for authors

+ IBR's and its stability properties are of great interest worldwide because of the continued deployment of IBRs at scale and because various instabilities (e.g., sub synchronous oscillations) have been observed in real systems. Therefore this paper studies an important and timely problem.
+ Many IBR stability analysis uses linear time invariant models. This paper focuses on nonlinear properties of GFM. Bifurcation behavior is important to understand and cannot be adequately studied using linear models. Therefore this paper fills a gap.

  Nonlinear systems are inherently much more difficult to analyze. There is often this tradeoff between (simplified) linear analysis that reveal structure properties around an equilibrium but may not be informative on global properties, or nonlinear analysis that covers global properties but is often too difficult to reveal much. Specifically:
- On the negatively side, the system studied is very simple, a single GFM connected to an infinite bus for a single set of nominal parameter values. The simulations of this simple system offer interesting insights, but it is unclear how these

properties might scale to bigger or more complex systems. In contrast, linear models in the literature are used to study large-scale networks of IBRs and practical grid codes.

- Simulation results often offer little structural understanding of the dynamic phenomenon. Such structural properties, especially properties that are scalable to larger or more complex systems, are often the most useful for design, operation and optimization of practical systems.

C. *Summarize your recommendation in one to two sentences*

The paper is marginal with strengths and weaknesses. I feel it adds useful insights, but I'm not familiar with the literature to judge how significant its relative contributions are. I hope other reviewers with more expertise can provide more information.

— *Anonymous reviewer*

III. Review #39C

A. *Paper summary*

The paper provides a bifurcation analysis of a grid-forming converter that reveal interesting stability bounds and spurious bifurcations that can arise from approximations.

B. *Comments for authors*

- The paper is easy to follow.
- The issue of continuation with ill-conditioned Jacobian needs a little more careful discussion than provided.
- The time-constants for the voltage and current controllers must be quite different to guarantee stability. Is there an easy way to explain why one would expect that?
- The effect of the smooth approximation of the current limiter is quite interesting. Again, is there any intuition that the authors can provide behind the spurious bifurcation obtained with smooth approximation?

C. *Summarize your recommendation in one to two sentences*

Accept.

— *Subhonmesh Bose*

IV. Brief response to reviewers (optional)

I would like to start by sincerely thanking the reviewers for lending their time and expertise in reviewing our manuscript. I will address here the primary discussion points raised in the comments. Comments that resulted in changes in the paper have been explained in the "brief summary of changes".

1) *Might we find similar modelling artefacts with other current limiting strategies?*
This is very interesting and is an area that requires further work. However, purely hypothesising, we might expect similar behaviour with axis priority limiters since these also sit between the inner voltage and current controllers (which participate in the mode of the spurious Hopf bifurcation). It is harder to speculate on the other methods listed by the reviewer but would be very interesting to see if their smooth approximations also cause any modes to go unstable (not just this inner voltage and current controller-related oscillation).
2) *Will we find similar results when analysing larger systems?*
We absolutely agree that it would be valuable to check whether such dynamics persist in multi-machine systems, although we were only focused on local phenomena in this work. From preliminary tests, we know that the strong grid Hopf bifurcation can still occur in multi-machine systems with heterogeneous generation devices, but have not yet tested whether the spurious Hopf bifurcations will still occur.
3) *Simulations offer little structural understanding of the dynamic phenomena.*
This is an important point and links to the need for more detailed analysis of the phenomena observed in this paper. However, it can be noted that the continuation approach used in the paper follows the equilibrium point, and so for each parameter value we are able to understand the system's underlying (linear) structure through eigenvalue analysis. For example, when a mode crosses into the unstable region (i.e., a bifurcation), we can use participation factors to understand better the states that are involved in that mode. In this paper it is an oscillation related to the inner voltage and inner current controllers of the GFM that goes unstable under the strong grid condition.
4) *Is there any intuition as to why the modelling artefact occurs?*
It is noted that the current limiter is placed between the inner voltage and current controller, both of which participate in the mode that (spuriously) goes unstable. However, more work is required to understand the impact of the smooth approximation, potentially utilising reduced order models to extract a closed-form expression for the oscillatory mode that goes unstable.

5) *Why must the voltage and current controller time constants be quite different to guarantee stability?*
   Our understanding is that this is a typical timescale separation issue. It is also known to be a particular problem in GFMs, especially in large power-rated scenarios when the switching frequency of a voltage-sourced converter must be reduced. This can result in interaction between the switching and the inner current controller. In our case, we see that the timescale separation issues are exacerbated in strong grid conditions.

V. Brief summary of changes made to the final paper

here were two minor changes made to the manuscript in response to the reviewer comments. The first was to explicitly state equations (14) and (15) for the circular current limiter; and the second was to improve the discussion on continuation failure near a saddle-node bifurcation point (e.g., removing the mention of eigenvalue sensitivities which was not pertinent to the discussion and only served to introduce ambiguity), along with the addition of reference [33] to support the explanation. An additional change has been made whereby mentions of ”discontinuous” action of the current limiter has been replaced by the term “non-smooth”. This is to reflect the fact that the current limiter is actually imposing a piecewise continuous action which is non-smooth. Finally, the heading of Section II-B has been changed from “Continuation of Equilibrium Branch” to “Continuation of Equilibrium Branch or Bifurcation Branch” to better reflect the content of the subsection.